

UC Berkeley

UC Berkeley Previously Published Works

Title

Inserting Porphyrin Quantum Dots in Bottom-Up Synthesized Graphene Nanoribbons

Permalink

<https://escholarship.org/uc/item/7c7367pg>

Journal

Chemistry - A European Journal, 23(70)

ISSN

0947-6539

Authors

Perkins, Wade
Fischer, Felix R

Publication Date

2017-12-14

DOI

10.1002/chem.201705252

Peer reviewed

Inserting Porphyrin Quantum Dots in Bottom-Up Synthesized Graphene Nanoribbons

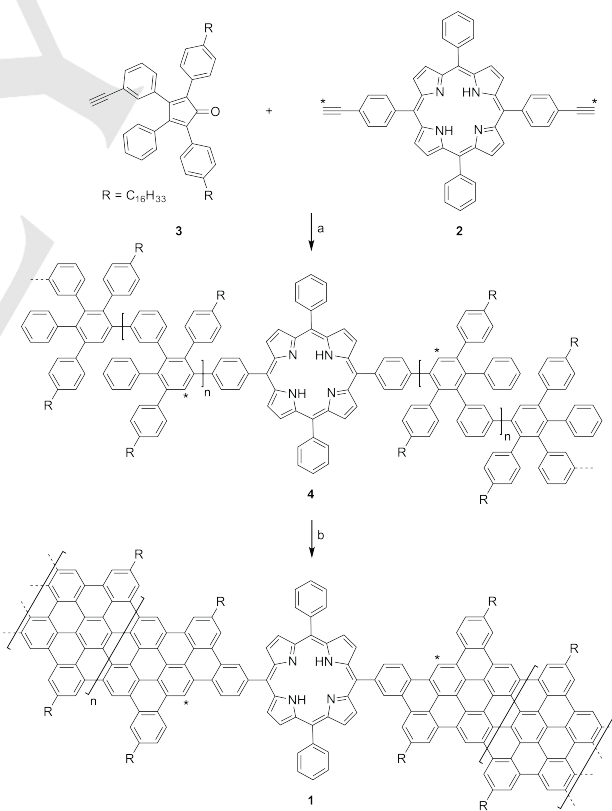
Wade Perkins,^[a] Felix R. Fischer^{[a,b,c]*}

Abstract: Diels-Alder copolymerization of tetrapheneylcyclopentadienone, a precursor for cove graphene nanoribbons (**cGNRs**), with bifunctional porphyrins yields defined nanostructures comprised of a single **cGNR**-porphyrin-**cGNR** heterojunction within each ribbon. ¹³C-NMR labeling and high-resolution mass spectrometry of solubilized polymer intermediates indicates that every porphyrin is covalently linked to two extended segments of **cGNRs**. UV-Vis absorption and fluorescence emission spectroscopy reveal a strong electronic correlation between the porphyrin and the adjacent **cGNR** segments that can be attenuated through reversible metalation of the porphyrin core. Our versatile bottom-up synthetic strategy provides access to structurally well defined, functional GNR-quantum dot-GNR heterostructures within a single graphene nanoribbon.

The design and implementation of carbon-based functional nanoelectronic materials into device architectures relies on the development of synthetic tools capable of providing a precise and reproducible control over the structure of materials at the nanometer scale. Recent advances in the bottom-up synthesis of semiconducting graphene nanoribbons (GNRs), quasi-one dimensional strips of single-layer graphene, have enabled the preparation of carbon-based nanomaterials with exquisite control over the width,^[1-5] the crystallographic symmetry (e.g. armchair,^[1-13] zig-zag^[14]), and the edge structure (cove,^[15-16] chevron^[1, 17-20]) both in solution and on metal surfaces. While bottom-up synthesized GNRs have been touted for their intrinsic exotic electronic,^[21-31] magnetic,^[25, 29-32] and optical properties,^[16, 27, 28, 33-34] examples for the deterministic assembly of functional bottom-up synthesized GNRs heterostructures have thus far been limited to uncontrolled copolymerization of molecular precursors on metal surfaces^[6, 13, 18, 20] or the study of small-molecule model systems in solution.^[35-37]

We herein report the solution-based bottom-up synthesis and characterization of a GNR heterostructure comprised of two segments of solubilized cove GNRs (**cGNRs**) linked by a substituted tetraphenylporphyrin core (**1**, Scheme 1) acting as a highly tunable molecular quantum dot (QD). While our synthetic

strategy can be extended to a variety of bifunctional linkers (see Supporting Information), we herein focus on the integration of a disubstituted tetraphenylporphyrin ($H_2(TPP)$) and its metal complexes into a **cGNR-H₂(TPP)-cGNR** heterostructure. Mass spectrometry (MS) and ¹³C-NMR spectroscopy of ¹³C-labeled poly-phenylene intermediates underscores the exquisite structural control over monomer sequence in the **cGNR-H₂(TPP)-cGNR** heterojunction. Electronic characterization of the resulting metalloporphyrin-**cGNR** hybrid materials by UV-Vis absorption and fluorescence emission spectroscopy shows strong electronic communication between the porphyrin and **cGNR** segments. We further demonstrate that reversible binding of primary amine ligands to the axial coordination site of the metalloporphyrin core can serve as a tool to direct the assembly of **cGNR-Zn(TPP)-cGNR** heterostructures on photolithographically patterned substrates.



Scheme 1. Synthesis of cove-type GNRs featuring a single porphyrin at the center of the ribbon. Reaction conditions: a) Ph_2O , 230 °C, 24 h, 40% b) $FeCl_3$, CH_2Cl_2 , CH_3NO_2 , 24 °C, 2 h, 55%. * 99.5% ¹³C isotopically labelled.

The deterministic bottom-up synthesis of **cGNR**-porphyrin-**cGNR** heterojunctions is depicted in Scheme 1. 5,15-bis(4-ethynylphenyl)-10,20-diphenylporphyrin (**2**) serves as the precursor for the porphyrin core in **1**. The solubilized **cGNR**

[a] W. Perkins, Prof. Dr. F. R. Fischer
Department of Chemistry,
University of California Berkeley
699 Tan Hall, Berkeley, CA-94720, U.S.A.
E-mail: ffischer@berkeley.edu

[b] Materials Science Division,
Lawrence Berkeley National Laboratory,
Berkeley, CA-94720, U.S.A.

[c] Kavli Energy NanoSciences Institute at the University of California
Berkeley and the Lawrence Berkeley National Laboratory,
Berkeley, CA-94720, U.S.A.

segments are derived from tetraphenylcyclopentadienone monomer **3**. Diels-Alder polymerization of **3** in the presence of **2** ($[3]/[2] = 24$) in Ph₂O at 230 °C yields the GNR polymer precursor **4** featuring a central porphyrin core extended on either side by chains of *poly*-**3** along with the expected homopolymer *poly*-**3**. Size exclusion chromatography (SEC) analysis of the crude polymer mixtures (calibrated to polystyrene standards) show a monomodal size-distribution centered around $M_n = 29000$, a polydispersity index $D_M = 1.8$, and an average degree of polymerization $X_n = 35$ (determined by ¹H-NMR end-group analysis of the characteristic porphyrin resonances at -2.8 ppm). Matrix-assisted laser desorption/ionization (MALDI) mass spectrometry (Figure 1a) reveals the presence of two distinctive families of polymers separated by $\Delta m/z = 662$ g mol⁻¹, the mass of the tetraarylporphyrin **2**. The repeat unit within both polymer families ($\Delta m/z = 829$ g mol⁻¹) corresponds to the mass of the monomer unit resulting from the Diels-Alder reaction and cheletropic extrusion of CO from **3**. To gain insight into the efficiency of the functionalization of both alkynes in the tetraarylporphyrin **2** we followed the copolymerization of **3** with 99.5% ¹³C labeled **2**. Characteristic ¹³C NMR resonances for the isotopically enriched terminal alkyne C-atom shift from $\delta = 79$ ppm in **2** to $\delta = 131$ ppm upon lateral extension of both ends of the porphyrin core with segments of *poly*-**3**. The absence of ¹³C labeled alkyne resonances ($\delta = 79$ ppm) in the crude polymerization mixture indicates that both functional ends of **2** have reacted and were efficiently incorporated into the extended polymer backbone. The crude polymerization mixture is thus comprised of only two distinctive polymeric species, the homopolymer *poly*-**3** and the copolymer **4** featuring a single porphyrin core extended on both sides by chains of *poly*-**3**.

Fractionation of the crude polymer mixture through column chromatography over SiO₂ yields *poly*-**3** and **4** in 45% and 40% isolated yield, respectively. While the MALDI mass spectrometry of *poly*-**3** (Figure 2b) shows only one characteristic family of peaks separated by the monomer mass ($\Delta m/z = 829$ g mol⁻¹), the corresponding MALDI of **4** (Figure 1c) contains predominantly (> 95%) the desired copolymer alongside trace amounts of *poly*-**3**. Figure 1d shows the aromatic region of the ¹³C NMR spectra of fractionated *poly*-**3** and copolymer **4**. The diagnostic resonance associated with the 99.5% ¹³C labeled terminal alkyne in **2** appears at $\delta = 131$ ppm. Oxidative cyclodehydrogenation of both *poly*-**3** and **4** with an excess of FeCl₃ gave solubilized **cGNR** and **cGNR**-porphyrin-**cGNR** heterostructure **1** in 96% and 97% isolated yield, respectively. Raman spectroscopy ($\lambda_E = 532$ nm) of fully cyclodehydrogenated **1** features characteristic radial breathing like mode (RBLM) (194 cm^{-1} FWHM = 78 cm⁻¹), D (1322 cm⁻¹ FWHM = 62 cm⁻¹), and G (1600 cm⁻¹ FWHM = 38 cm⁻¹) peaks with a ratio $I_D/I_G = 1.2$ reminiscent of pristine **cGNRs** along with higher order 2D, D+G and 2G peaks (Figure 2a).^[15] We conclude that the incorporation of a single porphyrin core at the center of a cove-type GNR does not perturb the structure of the parent **cGNR** segments in **1**.

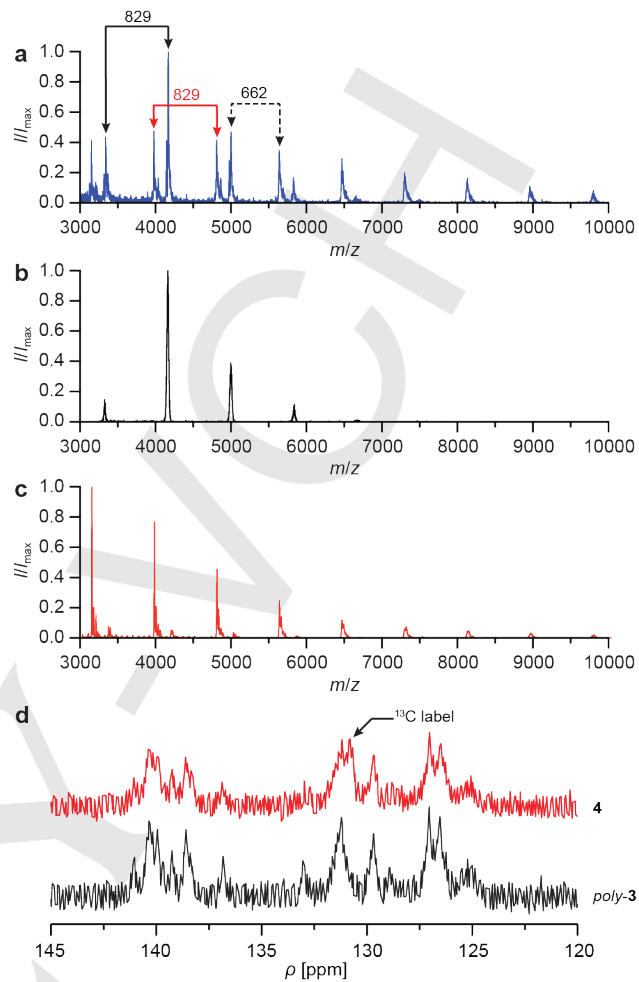


Figure 1. a) MALDI of crude polymer mixture containing *poly*-**3** and copolymer **4**. MALDI of b) purified *poly*-**3** and c) copolymer **4** fractionated through column chromatography. d) ¹³C NMR of purified *poly*-**3** (black) and copolymer **4** (red). The arrow indicates the characteristic resonance signal for the 99.5% ¹³C labelled aromatic carbon atoms resulting from the reaction of both terminal alkynes in **2** with **3**.

Both **cGNRs** and **cGNR-H₂(TPP)-cGNR** heterostructure **1** feature solubilizing hexadecyl side chains and form stable dispersions after sonication and centrifugation in THF. The respective UV-Vis absorption spectra are depicted in Figure 2b. A broad absorption at $\lambda_{\max} = 556$ nm characteristic for **cGNRs** dominates the spectrum of **1**. The λ_{\max} of **cGNR-H₂(TPP)-cGNR** heterostructure **1** is only slightly shifted (~6 nm) to shorter wavelength when compared to the absorption of pristine **cGNRs**. A second prominent absorption at $\lambda = 433$ nm in the spectrum of **1** can be attributed to the corresponding S₀→S₂ transition (Soret band) in the porphyrin core,^[38] while the characteristic Q-bands are obscured by the dominant absorption of the **cGNR** segments. The bathochromic shift (~10 nm) of the Soret band in **1**, when compared to the precursor **2** ($\lambda_{\max} = 423$ nm), can be attributed to an efficient electronic coupling with the extended π -system of the adjacent **cGNRs**. An inherent strength of porphyrins as the central component in functional GNR heterostructures is the ability to reversibly tune the electronic structure of the porphyrin through late-stage metalation. Coordination of Zn²⁺ ions to the

free-base porphyrin in **1** is mirrored in a diagnostic shift (~ 10 nm) of the Soret band to longer wavelengths (**1-Zn** in Figure 2b) (coordination of Ru^{2+} or Al^{3+} ions induces a negligible shift, Supporting Information, Figure 2SI). The complexation of Zn^{2+} is

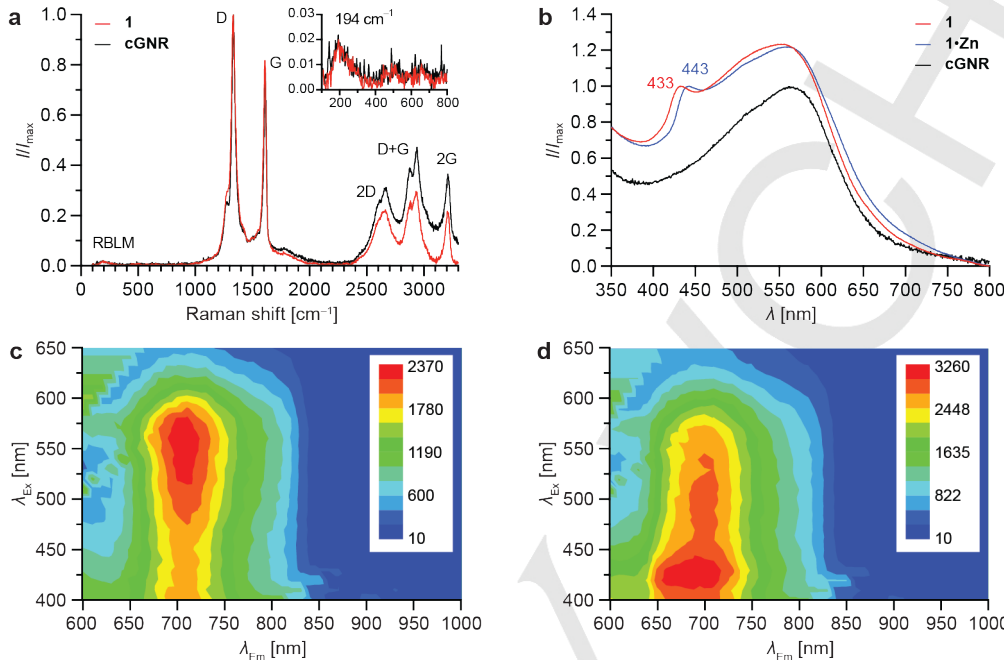


Figure 2. a) Raman spectra ($\lambda_{\text{Ex}} = 532$ nm) of pristine cGNRs and cGNR-H₂(TPP)-cGNR heterostructure **1**. Inset shows a magnification of a region of the spectrum associated with the radial breathing like mode (RBLM) at 194 cm^{-1} . b) UV-Vis spectra of dilute dispersions of cGNRs (black) (normalized to the absorption maximum of the GNR), **1** (red), and metallated **1-Zn** (blue) (normalized to the Soret band). EEM fluorescence spectra for c) cGNRs and d) cGNR-H₂(TPP)-cGNR heterostructures **1**.

Figure 2c,d shows the excitation emission matrix (EEM) fluorescence spectra for cGNRs and cGNR-H₂(TPP)-cGNR heterostructure **1**, respectively. Excitation of pristine cGNRs at $\lambda_{\text{Ex}} = 560$ nm leads to a broad fluorescence emission centered around $\lambda_{\text{Em}} = 705$ nm (Figure 2c). The emission of the cGNR-H₂(TPP)-cGNR heterostructure **1** upon excitation at the same wavelength ($\lambda_{\text{Ex}} = 560$ nm) decreases significantly (Figure 2d) and no longer represent the emission maximum. If, however the cGNR-H₂(TPP)-cGNR heterostructure **1** is excited at $\lambda_{\text{Ex}} = 425$ nm, close to the Soret band of the porphyrin core, a very broad emission $\lambda_{\text{Em}} = 650\text{--}720$ nm featuring emission characteristics of both the porphyrin and cGNR is observed. The energy transfer from the excited state of the porphyrin core ($\lambda_{\text{Ex}} = 425$) to the cGNR ($\lambda_{\text{Em}} = 705$ nm) further support an efficient electronic communication between the central porphyrin and the extended cGNR segments.

Axial coordination of a ligand to the metal in cGNR-Zn(TPP)-cGNR heterostructures can be used as a tool to direct the self-assembly of functional GNRs on patterned substrates. Figure 3a shows an Al₂O₃ substrate decorated with photolithographically

quantitative, reflected in a rigid shift of the Soret band, and is fully reversible. Treatment of **1-Zn** with trifluoroacetic acid in CH₂Cl₂ regenerates the free-base porphyrin **1**.

deposited Pt traces (Figure 3a). Self-assembled monolayer (SAM) of either *N*-(3-(triethoxysilyl)propyl)hexane-1,6-diamine (NH₂-SAM), or dodecyldimethoxysilane (CH₃-SAM) were selectively grown on the exposed Al₂O₃ substrate (NH₂-SAM and CH₃-SAM do not adhere to Pt traces). While the primary amine in NH₂-SAM can reversibly bind to metallated **1**, the CH₃-SAM serves as a reference to account for dispersion interactions between solubilizing alkyl chains in **1** and an aliphatic SAM. Figure 3b shows a representative Raman map of the G peak intensity attributed to **1-Zn** on a patterned substrate functionalized with NH₂-SAM. The spatial distribution of the Raman signature of **1-Zn** indicates that the interaction between the Zn²⁺ and the primary amine directs the assembly of **1-Zn** exclusively on the NH₂-SAM functionalized substrate. The significance of this selective metal ligand coordination is further supported by two control experiments. The spatial distribution of G peak intensity in Raman maps of **1-Zn** on CH₃-SAM (Figure 3c) or cGNRs on NH₂-SAM functionalized substrates (Figure 3d) do not indicate a preference for adhesion to the SAM over the photo lithographically patterned Pt traces.

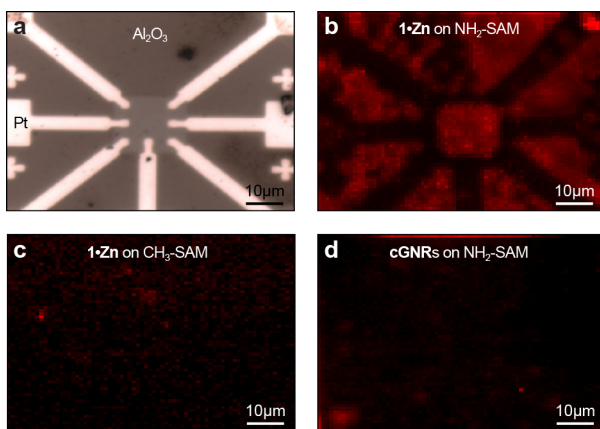


Figure 3. a) Optical microscopy image of Pt traces on a SAM functionalized Al_2O_3 substrate. Raman maps of the G peak intensity associated with **1-Zn** deposited on b) substrates functionalized with amine groups ($\text{NH}_2\text{-SAM}$) and c) substrates functionalized with hydrocarbon chains ($\text{CH}_3\text{-SAM}$). d) Raman map of **cGMR** deposited on a substrate functionalized with amine groups ($\text{NH}_2\text{-SAM}$).

In summary, we report the deterministic bottom-up synthesis of a GNR-QD-GNR heterostructure and its electronic characterization by UV-Vis and EEM fluorescence spectroscopy. Our synthetic strategy demonstrates that chains of a heteroditopic monomer can efficiently be fused by a single homoditopic linker. ^{13}C -NMR labeling experiments, MALDI-TOF MS and Raman spectroscopy confirm that only one linker molecule is incorporated at the center of the heterostructure. UV-Vis and EEM fluorescence spectroscopy reveal a strong electronic coupling between the **cGMR** segments and the central porphyrin. Besides tuning the electronic structure of the porphyrin core itself, metalation provides a secondary axial coordination site that can be used to direct the spatial localization of GNR-QD-GNR heterostructures through the interaction with amine terminated SAMs on photo lithographically patterned substrates.

Acknowledgements

Research supported by the U.S. Department of Energy, Office of Science, Office of Basic Energy Sciences, under Award # DE-SC0010409 Berkeley NMR Facility is supported in part by NIH grant SRR023679A.

Keywords: graphene • nanostructure • heterojunction • nanoribbon • porphyrin

- [1] J. Cai, P. Ruffieux, R. Jaafar, M. Bieri, T. Braun, S. Blankenburg, M. Muoth, A. P. Seitsonen, M. Saleh, X. Feng, K. Müllen, R. Fasel, *Nature* **2010**, *466*, 470–473.
- [2] Y.-C. Chen, D. G. de Oteyza, Z. Pedramrazi, C. Chen, F. R. Fischer, M. F. Crommie, *ACS Nano* **2013**, *7*, 6123–6128.
- [3] M. El Gemayel, A. Narita, L. F. Dossel, R. S. Sundaram, A. Kiersnowski, W. Pisula, M. R. Hansen, A. C. Ferrari, E. Orgiu, X. Feng, K. Müllen, P. Samori, *Nanoscale* **2014**, *6*, 6301–6314.

- [4] H. Zhang, H. Lin, K. Sun, L. Chen, Y. Zaganyarski, N. Aghdassi, S. Duhm, Q. Li, D. Zhong, Y. Li, K. Müllen, H. Fuchs, L. Chi, *J. Am. Chem. Soc.* **2015**, *137*, 4022–4025.
- [5] L. Talirz, H. Sode, T. Dumslaff, S. Wang, J. R. Sanchez-Valencia, J. Liu, P. Shinde, C. A. Pignedoli, L. Liang, V. Meunier, N. C. Plumb, M. Shi, X. Feng, A. Narita, K. Müllen, R. Fasel, P. Ruffieux, *ACS Nano* **2017**, *11*, 1380–1388.
- [6] Y.-C. Chen, T. Cao, C. Chen, Z. Pedramrazi, D. Haberer, D. G. de Oteyza, F. R. Fischer, S. G. Louie, M. F. Crommie, *Nat. Nanotechnol.* **2015**, *10*, 156–160.
- [7] R. R. Cloke, T. Marangoni, G. D. Nguyen, T. Joshi, D. J. Rizzo, C. Bronner, T. Cao, S. G. Louie, M. F. Crommie, F. R. Fischer, *J. Am. Chem. Soc.* **2015**, *137*, 8872–8875.
- [8] X. Yang, X. Dou, A. Rouhanipour, L. Zhi, H. J. Räder, K. Müllen, *J. Am. Chem. Soc.* **2008**, *130*, 4216–4217.
- [9] S. Kawai, S. Saito, S. Osumi, S. Yamaguchi, A. S. Foster, P. Spijker, E. Meyer, *Nat. Commun.* **2015**, *6*, 8098.
- [10] J. Gao, F. J. Uribe-Romo, J. D. Saathoff, H. Arslan, C. R. Crick, S. J. Hein, B. Itin, P. Clancy, W. R. Dichtel, Y.-L. Loo, *ACS Nano* **2016**, *10*, 4847–4856.
- [11] C. P. Sen, S. Valiyaveetil, *Chem-Eur. J.* **2017**, *23*, 1686–1693.
- [12] G. D. Nguyen, F. M. Toma, T. Cao, Z. Pedramrazi, C. Chen, D. J. Rizzo, T. Joshi, C. Bronner, Y.-C. Chen, M. Favaro, S. G. Louie, F. R. Fischer, M. F. Crommie, *J. Phys. Chem. C* **2016**, *120*, 2684–2697.
- [13] E. Carbonell-Sanromà, P. Brandimarte, R. Balog, M. Corso, S. Kawai, A. Garcia-Lekue, S. Saito, S. Yamaguchi, E. Meyer, D. Sánchez-Portal, J. I. Pascual, *Nano Lett.* **2017**, *17*, 50–56.
- [14] P. Ruffieux, S. Wang, B. Yang, C. Sánchez-Sánchez, J. Liu, T. Dienel, L. Talirz, P. Shinde, C. A. Pignedoli, D. Passerone, T. Dumslaff, X. Feng, K. Müllen, R. Fasel, *Nature* **2016**, *531*, 489–492.
- [15] A. Narita, X. Feng, Y. Hernandez, S. A. Jensen, M. Bonn, H. Yang, I. A. Verzhbitskiy, C. Casiraghi, M. R. Hansen, A. H. R. Koch, G. Fytas, O. Ivashenko, B. Li, K. S. Mali, T. Balandina, S. Mahesh, S. De Feyter, K. Müllen, *Nat. Chem.* **2014**, *6*, 126–132.
- [16] A. Narita, I. A. Verzhbitskiy, W. Frederickx, K. S. Mali, S. A. Jensen, M. R. Hansen, M. Bonn, S. De Feyter, C. Casiraghi, X. Feng, K. Müllen, *ACS Nano* **2014**, *8*, 11622–11630.
- [17] Y. Zhang, Y. Zhang, G. Li, J. Lu, X. Lin, S. Du, R. Berger, X. Feng, K. Müllen, H.-J. Gao, *Appl. Phys. Lett.* **2014**, *105*, 023101.
- [18] J. Cai, C. A. Pignedoli, L. Talirz, P. Ruffieux, H. Sode, L. Liang, V. Meunier, R. Berger, R. Li, X. Feng, K. Müllen, R. Fasel, *Nat. Nanotechnol.* **2014**, *9*, 896–900.
- [19] T. H. Vo, M. Shekhirev, D. A. Kunkel, M. D. Morton, E. Berglund, L. Kong, P. M. Wilson, P. A. Dowben, A. Enders, A. Sinitskii, *Nat. Commun.* **2014**, *5*, 3189.
- [20] T. Marangoni, D. Haberer, D. J. Rizzo, R. R. Cloke, F. R. Fischer, *Chem.-Eur. J.* **2016**, *22*, 13037–13040.
- [21] K. Nakada, M. Fujita, G. Dresselhaus, M. S. Dresselhaus, *Phys. Rev. B* **1996**, *54*, 17954–17961.
- [22] Y. Miyamoto, K. Nakada, M. Fujita, *Phys. Rev. B* **1999**, *59*, 9858.
- [23] K. Wakabayashi, *Phys. Rev. B* **2001**, *64*, 125428.
- [24] V. Barone, O. Hod, G. E. Scuseria, *Nano Lett.* **2006**, *6*, 2748–2754.
- [25] Y.-W. Son, M. L. Cohen, S. G. Louie, *Phys. Rev. Lett.* **2006**, *97*, 216803.
- [26] Y.-W. Son, M. L. Cohen, S. G. Louie, *Nature* **2006**, *444*, 347–349.
- [27] L. Yang, C.-H. Park, Y.-W. Son, M. L. Cohen, S. G. Louie, *Phys. Rev. Lett.* **2007**, *99*, 186801.
- [28] P. Ruffieux, J. Cai, N. C. Plumb, L. Patthey, D. Prezzi, A. Ferretti, E. Molinari, X. Feng, K. Müllen, C. A. Pignedoli, R. Fasel, *ACS Nano* **2012**, *6*, 6930–6935.
- [29] W. Han, K. Pi, K. M. McCreary, Y. Li, J. J. I. Wong, A. G. Swartz, R. K. Kawakami, *Phys. Rev. Lett.* **2010**, *105*, 167202.
- [30] W. Han, R. K. Kawakami, M. Gmitra, J. Fabian, *Nat. Nanotechnol.* **2014**, *9*, 704–807.
- [31] G. Z. Magda, X. Jin, I. Hagymasi, P. Vancso, Z. Osvath, P. Nemes-Incze, C. Hwang, L. P. Biro, L. Tapaszto, *Nature* **2014**, *514*, 608–611.

- [32] G. Cordouier-Maruri, Y. Omar, R. de Coss, S. Bose, *Phys. Rev. B* **2014**, *89*, 075426.
- [33] D. Prezzi, D. Varsano, A. Ruini, A. Marini, E. Molinari, *Phys. Rev. B* **2008**, *77*, 041404.
- [34] D. Prezzi, D. Varsano, A. Ruini, E. Molinari, *Phys. Rev. B* **2011**, *84*, 041401.
- [35] J. M. Englert, J. Malig, V. A. Zamolo, A. Hirsch, N. Jux, *Chem. Commun.* **2013**, *49*, 4827–4829.
- [36] D. Lungerich, J. F. Hitzenberger, M. Marcia, F. Hampel, T. Drewello, N. Jux, *Angew. Chem. Int. Ed.* **2014**, *53*, 12231–12235.
- [37] D. Lungerich, J. F. Hitzenberger, W. Donaubauer, T. Drewello, N. Jux, *Chem. Eur. J.* **2016**, *22*, 16755–16759.
- [38] J. B. Kim, J. J. Leonard, F. R. Longo, *J. Am. Chem. Soc.* **1972**, *94*, 3986–3992.

COMMUNICATION

The bottom-up solution-based synthesis and selective fractionation of graphene nanoribbon-porphyrin-graphene nanoribbon heterostructures is reported. Absorption and fluorescence spectroscopy reveal a strong coupling between the graphene nanoribbon and the central porphyrin quantum dot.



Wade Perkins, Felix R. Fischer*

Page No. – Page No.

Inserting Porphyrin Quantum Dots
in Bottom-Up Synthesized
Graphene Nanoribbons